Proceedings of the ASME 2020 39th International Conference on Ocean, Offshore and Arctic Engineering
OMAE2020
August 3-7, 2020, Virtual, Online

OMAE2020-18172

EXTREME VALUE ESTIMATION OF MOORING LOADS BASED ON STATION-KEEPING TRIALS IN ICE

Chana Sinsabvarodom*
NTNU
Trondheim, Norway

Bernt J. Leira
NTNU
Trondheim, Norway

Wei Chai
Wuhan University of Technology,
Wuhan, China

Arvid Naess
NTNU
Trondheim, Norway

ABSTRACT

The purpose of this work is to perform an extreme value estimation of the mooring loads associated with station-keeping of a ship operating in ice. In general, the design of mooring lines is based on estimation of the extreme loading caused by environmental conditions within the relevant area. In March 2017, station-keeping trials (SKT) in drifting ice were performed as part of a project headed by Statoil in the Bay of Bothnia. The objective was to investigate the characteristics of the mooring loads for the supply vessel *Magne Viking* for different types of physical ice management schemes. *Tor Viking* was employed as an ice breaker as part of the physical ice management systems. The ice conditions (i.e. the ice drift velocity and the ice thickness) during the trials were monitored by using Ice Profiling Sensors (IPSs). Different patterns of ice-breaking manoeuvers were investigated as part of the physical ice management systems, such as square updrift, round circle, circle updrift and linear updrift pattern were studied as part of the field experiments. The peak values of the mooring loads for the supply vessel are determined by using the min peak prominence method. For the purpose of extreme value prediction, the peak over threshold method and block maxima method for a specific time window are applied to estimate the mooring loads that correspond to specific probabilities of exceedance (or equivalently: return periods). These loads can then be compared to the design loads that are being specified by relevant international standards.

Keyword: station-keeping trials; Ice loads; extreme values

NOMENCLATURE

ADCP	Acoustic *Doppler current profiler*
BM	*Block maxima*
MBL	*Minimum breaking load*
IM	*Ice management*
IPS	*Ice profiling sensor*
MV	*Magne Viking*
POT	*Peak over threshold*
SKT	*Station-keeping trials (in ice)*
SWL	*Safe working load*
TV	*Tor Viking*
ULS	*Upward looking sonar*

INTRODUCTION

Increasing offshore activities in the Arctic region also imply an increasing number of marine operations in this area. Accordingly, the ability to predict ice loads and corresponding load effects on stationary ship structures in a precise way will be essential with respect to safety, integrity, cost efficiency and regularity of such operations. However, data from different full-scale testing scenarios for stationary floating structure is limited, and even less are publicly available. In order to collect more relevant data, Statoil conducted station keeping trials (SKT) in drifting ice in the Bay of Bothnia in March 2017. Two anchor handling and tug vessels, *Magne Viking (MV)* and *Tor Viking (TV)* were applied in order to obtain the full-scale measurement. An overview of the different parts of the SKT project is given in [1]. Traditionally, numerical simulations and Ice basin tests have been employed in order to study ice actions and structural responses due to sea ice. However, the numerical simulations still require further research in order for them to be validated. Not the least, such validation should be based on full scale tests [2].

Furthermore, the ISO 19906 standard allows design methods based on full-scale measurements in order to quantify the ice parameters and design ice loads for offshore structure[3]. Typically, for permanent mooring systems both overloading and fatigue are of primary concern [4]. The present study is mainly concerned with design against overloading, and accordingly analysis of extreme mooring loads is in focus. For offshore

operations in cold regions, the associated low temperatures can enhance the hardness of steel materials, which contributes to fatigue endurance [4]. In case of mobile units, only analysis for extreme response is required for the mooring system [5]. For the ultimate limit state (i.e. overload), design with respect to an extreme tension load effect with a certain return period is in general required[3, 6].

Hence, the aim of the present study is to estimate the extreme mooring loads based on full-scale measurements during station-keeping trials (SKT) in drifting ice. Different management schemes under the different ice conditions [7] are considered in order to estimate short-term extreme mooring loads. Extrapolation to long-term extreme loads is also discussed.

ICE MANAGEMENT

Ice management generally involves various operational procedures so as to reduce the ice action on various types of offshore structures [8, 9]. For the present full-scale experiment, various types of ice management schemes are applied in relation to the station keeping trials for various ice conditions. Traditional ice management schemes have been based on circular or some form of elliptical pattern. Such patterns allow the icebreaker to maintain a relatively high/effective speed for most ice conditions. Positive experience with such a scheme is reported by several operators. Circular and elliptical patterns are preferable since they are effective, and relatively easy to use[10]. For some other patterns, i.e. the square pattern abrupt turns are required which are difficult to achieve, especially during the first cut of unbroken sea ice.

(a) Tor Viking

(b) Magne Viking

Fig.1 Pictures of supply vessel and icebreaker [10]

In the present full-scale experiments two vessels are involved i.e. one ice-breaking vessel and one stationary supply vessel. The first vessel is the Tor Viking (*TV)* as shown in figure 1a, for which the class notation is ICE-10 icebreaker. This vessel was built by Kvaerner Leirvik in the year 2000. The major role of *TV* was to provide ice management and anchor handling support for the stationary vessel *MV* which is shown in figure 1b. The class notation of *MV* is DNV ICE-1A. It was built by Astilleros Zamakona in the year 2011. The dimension of both two vessels are given in [11].

Four patterns of the ice management applied during the full-scale trials are illustrated in figure 2. The corresponding measurement records are presently analyzed in order to estimate the extreme mooring forces. There are the different pros and cons for each pattern relatively owning to the many factors i.e. the ability of the icebreaker, weather condition, visualization, ice conditions etc. Before the hand, the selected ice management pattern can be maintained by using the ship's Electronic chart display and information system (ECDIS) to plan the route of the ice breaker. This tool is very usual full and effective, especially during the period of the low visibility [10]. Since the relative low maneuverability of the *TV* in the level ice. The most challenge part of the ice management became the initiating pattern. Especially, the first loop is the most difficult as the ice is unbroken. Therefore, the speed of the vessel was relatively low in the first turn, which takes relatively long time in order to make the first pass compared to subsequent passes.

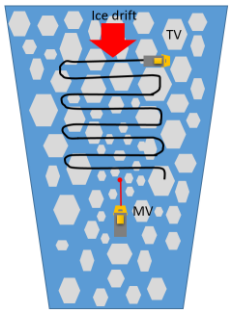

(a) Case 1: Square updrift tracks

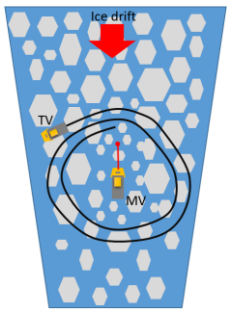

(b) Case 2: Round circle track

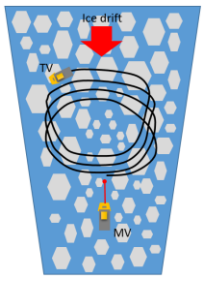

(c) Case 3: Circle updrift tracks

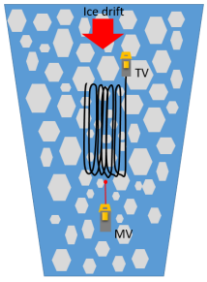

(d) Case 4: Linear updrift track

Fig.2 Patterns of ice management schemes applied during full-scale tests

The first pattern is the square updrift track (relative to) MV as shown in figure 2a. This pattern is based on straight-line motion, which allows the vessel to increase the speed before making sharp 90 degree turns at the transition points. However, the combination of high speeds and sharp turns associated with the square pattern can cause excessive roll of the vessel. The second pattern is the round circle track as illustrated in figure 2b. It is suitable for the range of low drift speed in order to minimize the outgoing floe size and produce a large quantity of brash. Third pattern is the circle updrift track as shown in figure 2c. The circular approach can be resumed the ice floes being broken. It is easily pushed the ice into the previous track, which is significant reduction turning resistance. Therefore, the higher speeds typically about 10-12 knots were achieved after the ice management was initialized. The circular approach is the most effective and preferable in the most condition experienced during the trials, except when the ice drift was relatively high and the ice was relatively severe[10]. Fourth pattern is the linear updrift

track as illustrated in figure 2d. It is the novel pattern that had been implemented in IM operation for station-keeping trials in ice.

The full-scale ice management tests were performed during different days. The weather forecast was applied in order to predict the weather and ice conditions before planning the test. Several tests were performed during the project [1]. The time table of the full-scale measurement for each pattern of ice management operation is listed in the table 1. The schedule is slightly different with the planning. This research, the time schedule in the table is based on the real time record of TV's track when it started and finished the IM operations.

Table 1- The schedule for each pattern of IM operations

IM operation	Date	Time
Square updrift pattern	9-Mar 2017	11:00:00 –13:25:00
Round circle pattern	12-Mar 2017	10:00:00 –14:25:00
Circle updrift pattern	16-Mar 2017	19:40:00 –21:40:00
Linear updrift pattern	16-Mar 2017	21:40:00 –00:30:00

WEATHER CONDITIONS

The met-ocean conditions during the field experiment were recorded, such as air temperature, wind speed, wind direction, ice draft, ice drift speed, ice concentration etc. Four ice profiler measurement systems were installed and moored to the seabed. The location of these four measurement stations are given in [7]. The ice profilers, which installed at the mooring buoys was typically resided approximately 35 - 45 m below the water surface. The IPSs are utilized to measure ice draft so as to obtain an estimation of the ice thickness as well as the ice ridges. The acoustic Doppler current profilers (ADCP) is deployed to measure the ice drift speed and direction. The detail of met-ocean condition is given in [7]. The general data of met-ocean during the testing date are listed in table 2.

Table 2- Summary of met-ocean data during the tests [12]

Item	Pattern (**a**)	Pattern (**b**)	Pattern (**c**)	Pattern (**d**)
	9-Mar	12-Mar	16-Mar	16-Mar
Level ice thickness, m	0.25-0.40	0.25-0.5	0.5-0.6	0.5-0.6
Rafted ice thickness, m	0.5-0.8	0.5-1.0	0.7-1.10	0.7-1.10
Ice ridges (width/height), m	Nil	10/1 -2	5/1-2	5/1-2
Ice drift speed, m/s	0.1-0.3	0.06	0.1	0.1
Ice floe size (intact), m	100 - 1000	100-1000	100-1000	100-1000
Ice concentration, th	9-10	9-10	9-10	9-10
Ice pressure (Rus scale)	1	1	1	1
Ice salinity, ppt	0.5	0.6	0.6	0.6
Sea water density, kg/m3	1002	1002	1002	1002
Wind speed, m/s	8 - 15	4-7	8-11	8-11
Wind direction, deg	190	230	280	280
Visibility, nm	0.5 - 3.0	20-40	20-30	20-30
Air temperature, deg C	-2 to -0	-1 to 0	-1 to +3	-1 to +3
Sea water temperature, deg C	-0.3	-0.4	-0.4	-0.4
Comp strength, MPa	3.8	3	2.5	2.5
Flex strength, MPa	0.7	0.5	0.5	0.5

The ice draft measured by the IPSs and the ice drift speed measured by the ADCP are shown in figure 3. The drift speed of the ice is highest during the test with pattern 1: the square updrift tracks. The drift speed of the ice lowest during the test with pattern 2: the round circle track. In the pattern 4, the drift speed is more fluctuated during the test. The mean values of the ice drift speed for each tests are 27, 6, 18, and 16 cm/s, respectively.

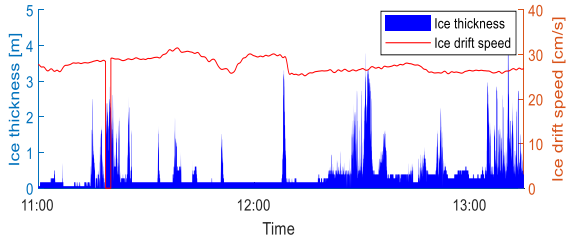

a) Ice thickness and ice drift speed during square updrift breaking pattern

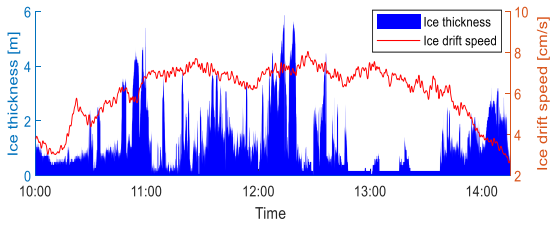

b) Ice thickness and ice drift speed during the round circle breaking pattern

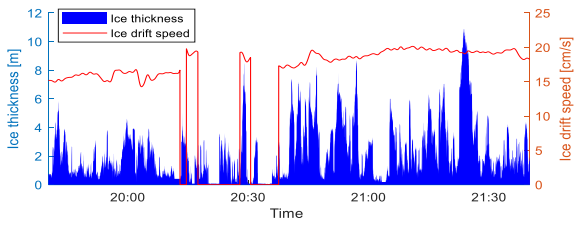

c) Ice thickness and ice drift speed during the circle updrift breaking pattern

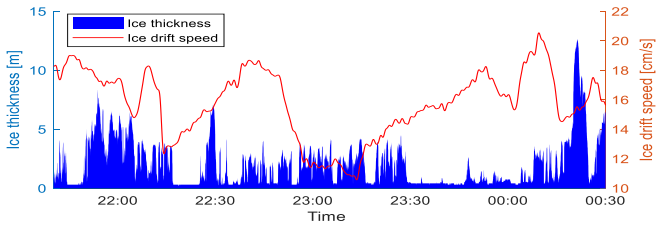

d) Ice thickness and ice drift speed during linear updrift breaking pattern

Fig.3 Ice draft and ice drift speed during the full scale measurement of mooring loads [13]

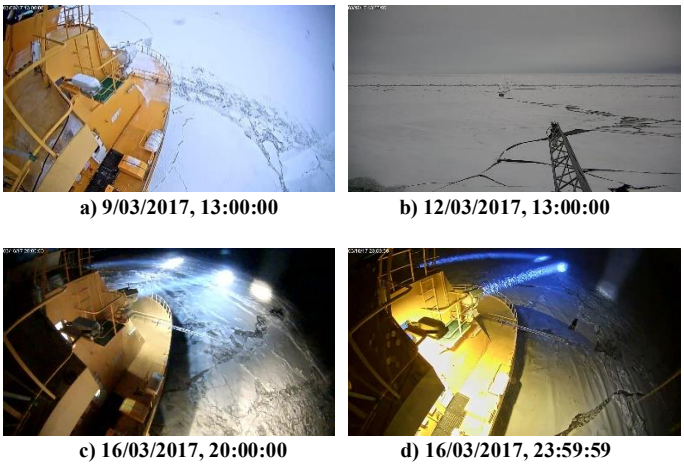

a) 9/03/2017, 13:00:00 **b) 12/03/2017, 13:00:00**

c) 16/03/2017, 20:00:00 **d) 16/03/2017, 23:59:59**

Fig.4 Images from camera records at *MV* during the full-scale test[13]

Moreover, the cameras are also utilized in order to record the ice surface around the supply vessel, *MV*. Altogether 15 cameras were install in order to record the images once a second. The visual images are not only utilized to estimate the average size of the ice floes ,but they can also be used in order to estimate the ice drift velocity around the supply vessel [14]. Furthermore, the pictures serve to visualize the characteristics of the surrounding environments such as surface snow cover (provided there is sufficient light for the cameras to work). Furthermore, due to wind snow may stick to the camera lenses, which can cause the pictures to be more or less blurred. Figure 4 provides some illustration of the ice surfaces in front of MV in the direction of the incoming ice drift for each of the four different test periods.

MOORING LINE SYSTEM

The tension in the mooring line was measured during the full-scale experiments by means of a load cell, which was connected between the bow of *MV* and the mooring chain as illustrated in figure 5. The load cell is of the Vetek D200 type, which is based on a hard-wired strain-gauge and with a safe working load (SWL) of 150 tons (±0.1%) [15]. The mooring equipment was rented from ISO Intermoor, and the details of the mooring and anchor system are given in [11].

The steel wire which constitutes a section of the mooring line has a minimum breaking loads, 223 Ton. It is intended as a weak link/ultimate load barrier and will break if the loads exceed the operational limit in the case of an uncontrollable situation. For emergency disconnection of the mooring line, a hydraulic wire cutter was installed in the weak link section close to the mooring attachment point on the forecastle deck of *MV*.

(a) Location of load cell in the mooring line [15]

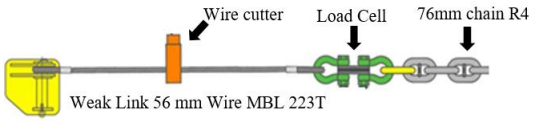

(b) Mooring connection arrangement [11]

Fig.5 Location of the load cell for monitoring of mooring loads

LOADING MECHANISM AND PEAK DETECTION

The time variation of the mooring load will clearly depend on the corresponding time variation of the ship-ice interaction process, and this applies in particular to the ice breaking process. The time series of the measured ice induced mooring loads generally consists of a sequence of impulses with quite sharp peaks [16]. The ice-induced loading process can be split into three distinct stages, i.e. the approaching stage, the crushing stage and the disengaging stage [16]. During the full-scale experiments, the ice concentration was very high, i.e. at a level of approximately 9.5 out of 10. For the periods with the highest ice concentrations, the approaching stage of the ice-induced mooring load is of very short duration as illustrated in figure 6.

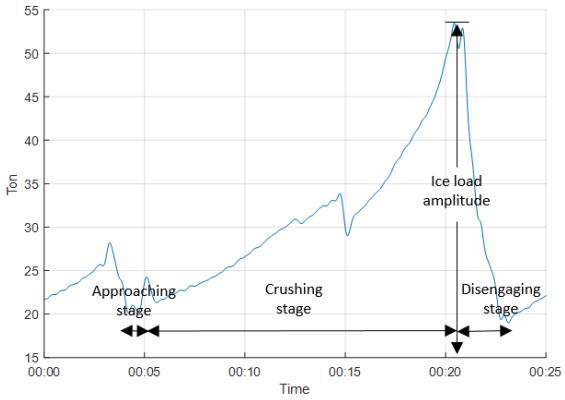

Fig.6 Three stages of the ice load generation process

The three-stage process of the mooring load will be continuously repeated when the ship hull encounters successive ice edges.

The peaks of the mooring line loads are determined by using the peak prominence method from the Matlab toolbox [17]. This method is based on the shorted vertical distances from the lowest neighboring valley to each peak. The peak prominence method can be applied in order to avoid that small peaks caused by signal noise are included as part of the recorded time series. An example of a sequence of peak detections by means of this method is illustrated in figure 7. The peak amplitudes of the mooring load are next employed in order to perform extreme value distributions.

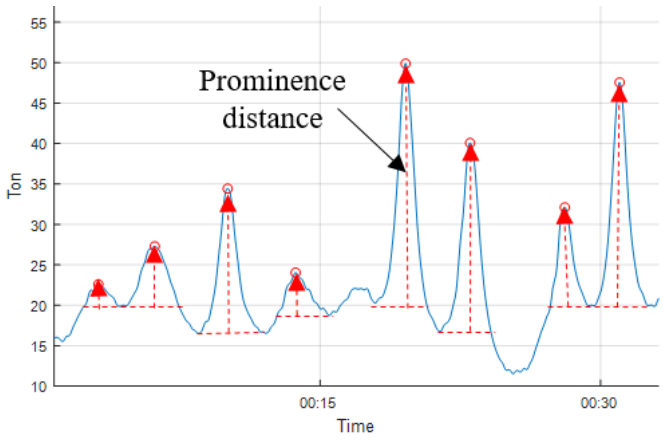

Fig.7 Example of the process for peak prominence detection.

EXTREME VALUE PREDICTION

The peak mooring loads from the full-scale measurement are represented by a random variable in order to perform an extreme value analysis. The sample values of the peak loads, i.e. $X_1,...,X_N$, are assumed to be independent realizations of the same underlying variable with a given probability distribution. This initial distribution function, $F(x)$ can be used to establish the extreme value distribution [18] for η, which is the largest value among in a sample of size N :

$$P(\eta) = \text{Prob}(X_1 \le \eta,...,X_N \le \eta) \tag{1}$$

According to the assumption of independence and identically distributed outcomes, equation 1 can be rewritten as given in equation 2:

$$P(\eta) = \prod_{i=1}^{N} \text{Prob}(X_i \le \eta) = \left[F_X(\eta)\right]^N \tag{2}$$

where N is the number of ice load peak events for the specific period under consideration.

The extreme value distribution can be determine by means of different approaches. In the present study, two approaches for this purpose. The first method is the peak over threshold method (POT). The peak data points which exceed a certain threshold are then fitted by an extreme value distribution function. The formulation for the extreme value analysis by the POT method is described e.g. in [19, 20].

The second method is the block maxima (BM) method, for which the largest peak of the mooring load within time windows of a fixed duration. These peaks are then applied in order to fit the initial distribution, $F(x)$. This fitted distribution is then inserted in equation (2) in order to arrive at the extreme value distribution.

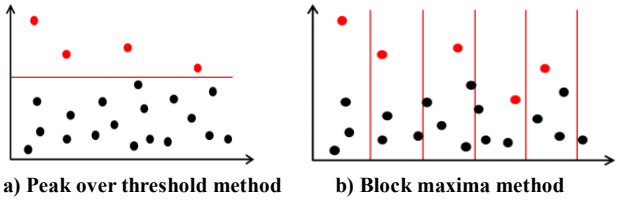

a) Peak over threshold method **b) Block maxima method**

Fig.8 The concept of peak over threshold and block maxima method (https://kturnbullblog.wordpress.com/)

For the block maxima method, the extreme value corresponding to a specific exceedance probability level, λ, is given in equation 3. Here, N denotes the number of blocks into which the measurement record is divided:

$$\eta = F^{-1}\left[(1-\lambda)^{1/N}\right] \tag{3}$$

For the short-term extreme mooring loads in the connection with experimental duration, the relationship between exceedance probability, λ and return period measured by number of days, T_{day} is given in equation 4. Here, T_{test} is the duration of a given full-scale test measured in number of hours. R is a reduction factor due to the operation frequency (i.e. the time in operation divided by the total time).

$$\lambda = \frac{1}{\frac{24}{T_{test}} \cdot R \cdot T_{day}} \tag{4}$$

The Gumbel distribution is much applied in connection with extreme value analysis. The equations for the cumulative distribution function (CDF) and the probability density function (PDF) are given in equation 5 and 6.

$$F_G(x) = \exp\left\{-\exp\left[-\left(\frac{x-\beta}{\alpha}\right)\right]\right\} \tag{5}$$

$$f_G(x) = \frac{1}{\alpha}\exp\left(\frac{x-\beta}{\alpha}\right)\cdot\exp\left\{-\exp\left[-\left(\frac{x-\beta}{\alpha}\right)\right]\right\} \qquad (6)$$

where β and α are the location and scale parameters, respectively. These parameters can be estimated e.g. by using least square fitting in a probability paper, by the method of moments or by the maximum likelihood method.

RESULTS AND DISCUSSION

For the full-scale station-keeping trials (SKT) in drifting ice, the icebreaker, *TV* is employed for the purpose of ice management. The ice was broken in the updrift direction relative to the stationary supply vessel, thus reducing the ice loads on this vessel. The ice drift behavior was monitoring by two types of instruments with the local station by ADCP measurement and ice drift beacon, which installed on the sea ice [7]. During the IM operations, the ice rose diagram can be applied to demonstrate the ice drift speed and directions [21]. The traveling tracks of icebreaker and supply vessel for each pattern scheme during IM operations in the latitude and longitude angles are shown in figure 9. Four different schemes for ice management are studied. The real tracks of the icebreaker during each IM operation are slightly different from the planned one due to variation of ice thickness, ice drift speed and the ice capabilities of the icebreaker.

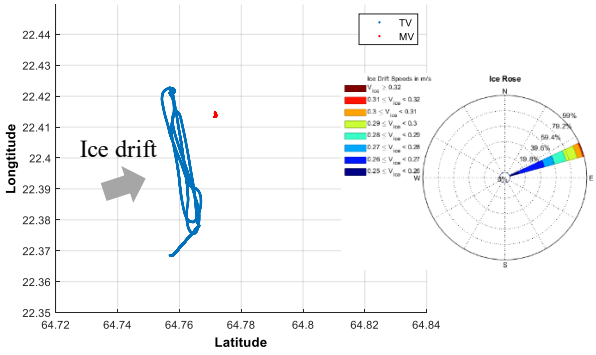

(a) Case 1: Square updrift tracks

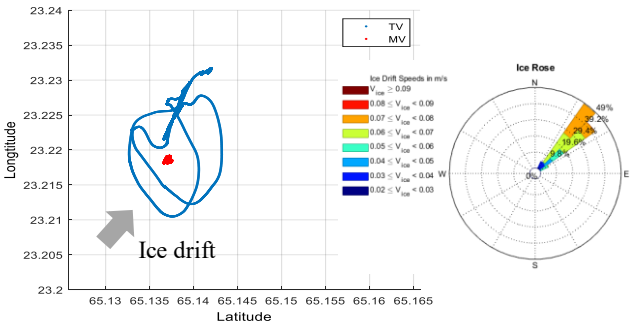

(b) Case 2: Round circle track

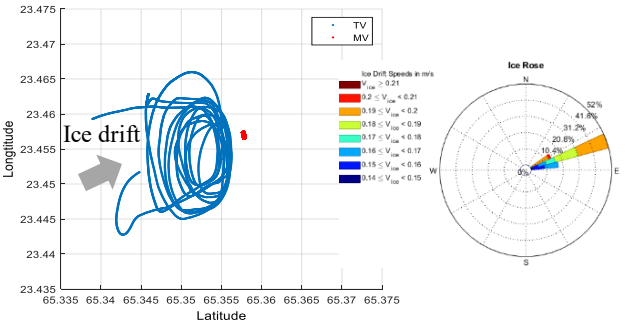

(c) Case 3: Circle updrift tracks

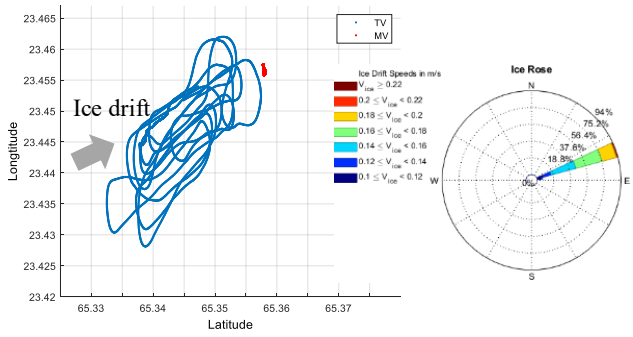

(d) Case 4: Linear updrift track

Fig.9 Trajectory of TV and MV during the IM operations for station-keeping trials in drifting ice

Time series of mooring loads during each of the ice management operations are provided by the load cell with one recording every second. The peak loads of the mooring line were computed by using the peak prominence method in order to avoid the local peaks caused by signal noise. The value of the minimum prominence for peak detection was set equals to 2 ton in the analysis. The results of the peak detection in the time series of the mooring load for different cases of IM operation are shown in figure 10.

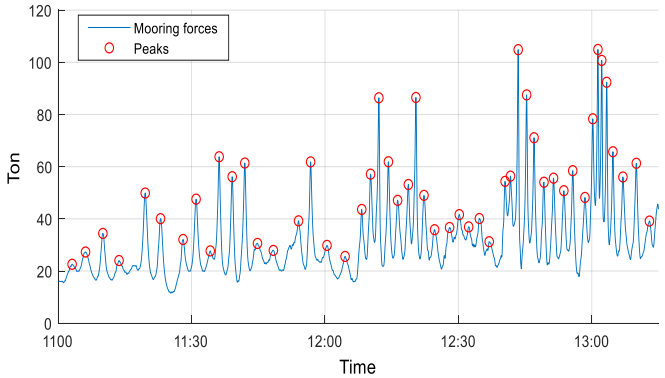

(a) Case 1: Square updrift tracks

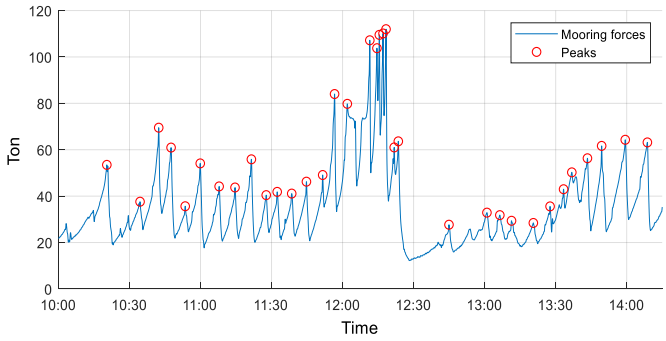

(b) Case 2: Round circle track

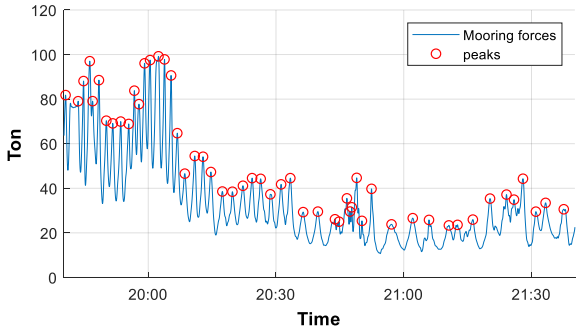

(c) Case 3: Circle updrift tracks

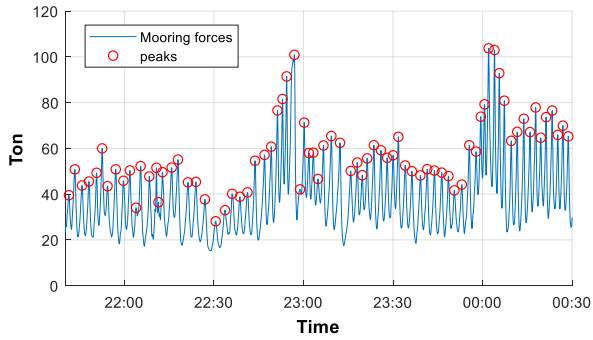

(d) Case 4: Linear updrift track

Fig.10 Mooring forces for different IM schemes

The peak values of the mooring load time series are used to perform the short-term extreme value analysis. The results of extreme mooring loads estimated by the peak over threshold (POT) method and the block maxima (BM) method were compared. The peak data points for the BM method were fitted to various probabilistic models in order to determine the initial distribution (or parent distribution) to be applied for the extreme value analysis. Subsequently, the Gumbel distribution was found to provide the most appropriate fitting of the extreme mooring load peaks for both POT and BM methods. Examples of fitting the peak mooring loads by the Gumbel distribution for both the POT and BM methods for the case with the Square updrift pattern are illustrated in figure 11 and 12, respectively.

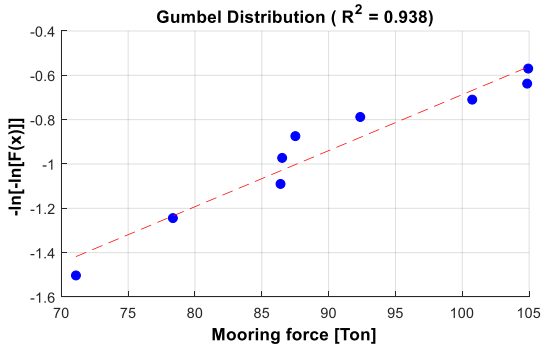

Fig.11 Example of data fitting for the extreme distribution by peak over threshold method

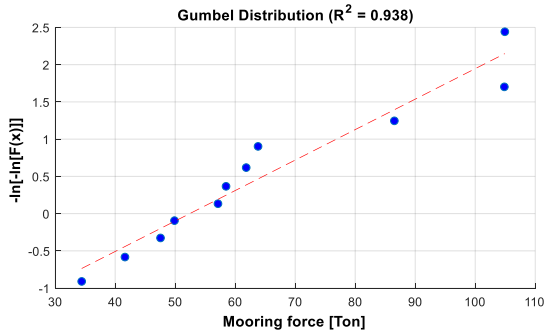

Fig.12 Example of data fitting for the initial distribution by the block maxima method

It is found that the extreme mooring load distribution obtained by the POT and the BM methods are sensitive respectively to the applied value of the threshold and to the length of the time window. Examples of extreme mooring load PDFs obtained by varying the threshold value for case 3 are illustrated in figure 13. The proper threshold value to be applied by the POT method needs careful consideration since higher threshold values will result in a smaller and smaller number of data points to be applied for the fitting.

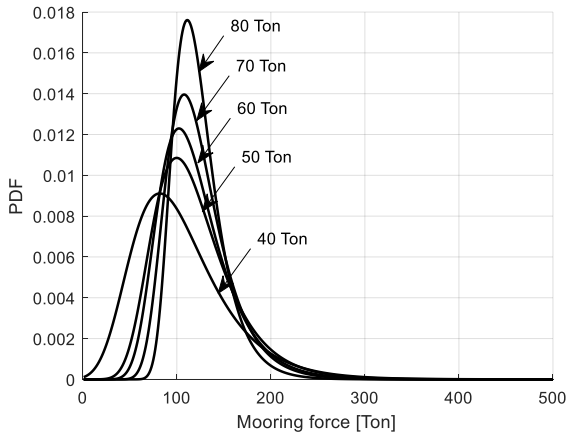

Fig.13 Examples of extreme mooring load PDFs by varying the threshold values for the POT method for the case with circle updrift pattern

For the BM method, the duration of the time window can be selected within the range from approximately 5 to 25 minutes. The time window for extreme mooring analysis is longer than the time window for the extreme ice loads on the ship hull itself, which is typically about one-five minutes [16, 22]. This is due to the peak mooring loads being caused by the integrated effect of all the local ice loads acting on the ship hull. This causes the interval between the mooring load peaks to be longer than the interval between the local ice load peaks. Examples of sensitivity studies with respect to the duration of the time window for the BM method (for case 3: circle updrift pattern) are illustrated in figure 14.

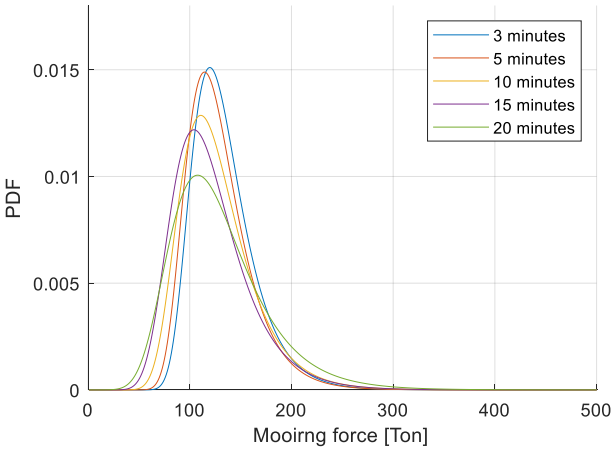

Fig.14 Examplex of extreme mooring load PDFs by varying the threshold values for the BM method (for the case of circle updrift pattern)

The location and shape parameters of the Gumbel extreme value distribution obtained by the POT and BM methods are listed in table 3.

The PDFs of the extreme peak loads obtained by the POT method tend to provides higher values than the BM method, but with case 3 being an exception. Suyuthi, Leira and Riska [22] also performed extreme value estimation by using the initial distribution for the peak loads and applying the number of peak data points equal to the parameter, N in equation 2. This provides extreme load distributions close to those obtained by the BM method.

A comparison of extreme mooring load PDFs obtained by the POT and BM methods for each pattern of IM operations is shown in figure 15.

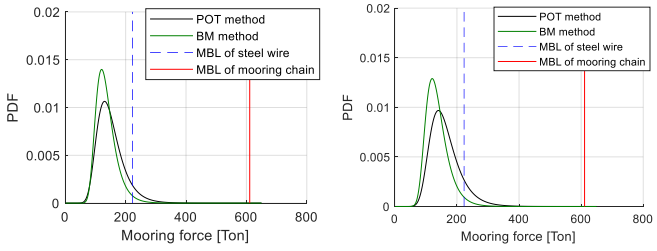

(a) Case 1: Square updrift pattern **(b) Case 2: Round circle pattern**

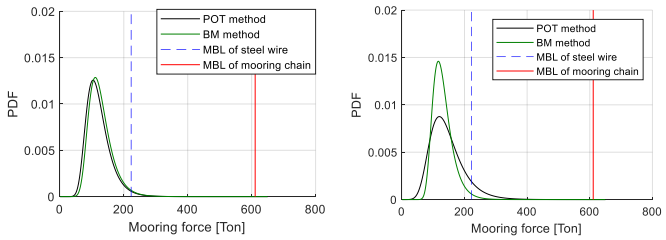

(c) Case 3: Circle updrift pattern **(d) Case 4: Linear updrift pattern**

Fig.15 Comparison of extreme mooring load PDFs obtained by the POT and BM methods for each pattern of IM operations

	Peak over threshold (POT)			Block maxima (BM)			
	Threshold (Ton)	Location parameter	Scale parameter	Time window (minutes)	Numb. of block	Location parameter	Scale parameter
Case 1	80	130.227	34.569	15	11	133.922	26.307
Case 2	83	140.362	38.009	15	17	116.748	28.527
Case 3	65	103.899	29.261	10	12	105.670	28.600
Case 4	68	119.723	41.997	25	6	148.651	25.197

Table 3- The shape and location parameters of the Gumbel distribution for extreme value analysis by the POT and BM methods

During the full-scale measurements, the mean values and standard deviations of the level ice thickness, the ice draft and the ice drift speed are recorded as shown in figure 16, 17 and 18, respectively. The statistical parameters of the level ice thickness and the ice raft/ridges were calculated from the recorded IPS time series. However, the records of ice draft from the IPS is unable to distinguish between level ice thickness, consolidated layer or ice rubble. Therefore, the maximum values of the last ten years from drilling data related to level ice thickness [23] in the Bay of Bothnia were used to distinguish between the data pertaining to the level ice thickness and ice raft/ridge in the time series.

The maximum level ice thickness and ice draft occurred during the IM operations in case 3 and 4, respectively. The highest ice drift speed occurs during case 1: square updrift pattern, while the ice thickness and ice draft had the lowest mean values for this case.

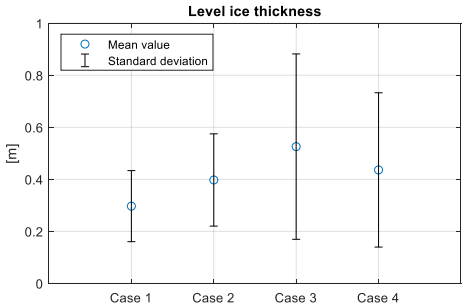

Fig.16 The level ice thickness during ice management operations.

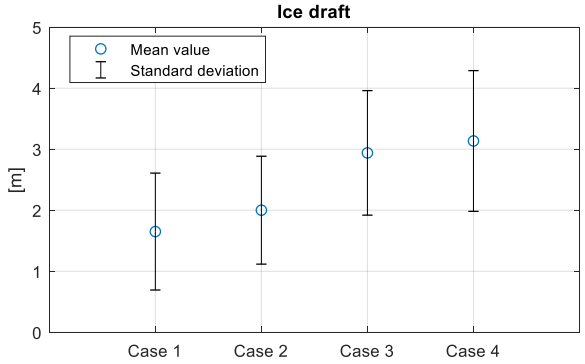

Fig.17 The keel of ice raft/ridge during ice management operations.

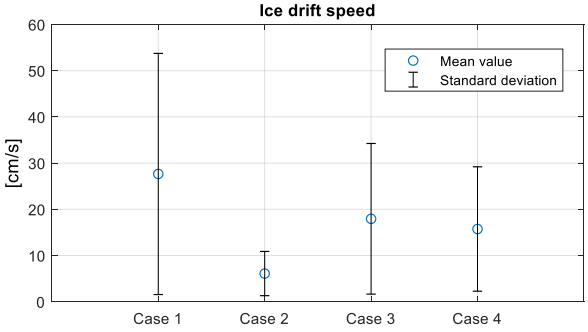

Fig.18 Ice drift speed during ice management operations.

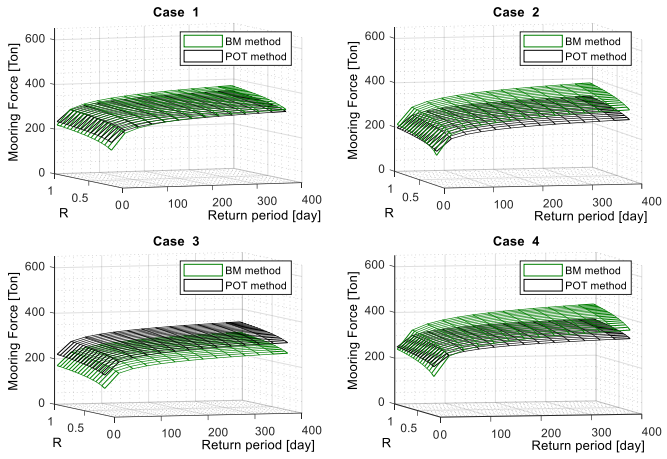

Fig.19 Comparison of extreme mooring force estimated by different methods corresponding to the return period and reduction factor, *R*

The results for the short-term extreme mooring loads obtained by the POT and BM methods are in good agreement. Both methods provide the same trends for the extrapolated long-term extreme mooring loads corresponding to the return period and reduction factor, *R* for each IM operation as illustrated in figure 19. The maximum difference between the long-term extreme mooring loads obtained by the two method is approximately 15 percent.

According to offshore standard for general marine operation by DNV-OS-H101[24], the accepted return period for design of marine operation depends upon the reference period in the field operation. In this experiment, a one-week operation was considered for the full-scale mooring test (not including installation, dynamic positioning test and other tests). The minimum accepted design return period for a one-week operation is three months, which were used in short-term extreme value analysis. However, it should also be kept in mind that this offshore standard was originally developed for operations in open water.

For a three months return period and reduction factor, *R* of operation frequency with 0.375, case 4 (with the linear updrift scheme) tends to provide the highest extreme mooring forces with 320 ton and 298 ton for the POT and BM methods, respectively. This is higher than the capacity of the load cell (150 ton) and the minimum breaking load, (MBL = 223 ton) of the steel wire.

The minimum extreme mooring load occurred for case 3: the circle updrift pattern with estimates of 227 ton and 274 ton for the POT and the BM methods, respectively.

The efficiency of the different ice management schemes were quantified by considering the ratio between the ice thickness/draft and extreme mooring loads as illustrated in figure 21. It is found that case 1: square updrift pattern and case 2: round circle pattern provide the lowest efficiencies of the IM operations. Moreover, during case 2, the thrusters of the supply vessel, *MV* were also applied in order to support the mooring system, which the weakest link at the load cell has the maximum capacity about 150 ton as illustrated in figure 20. However, only the mooring loads for case 2 are employed for the purpose of short-term extreme mooring load analysis.

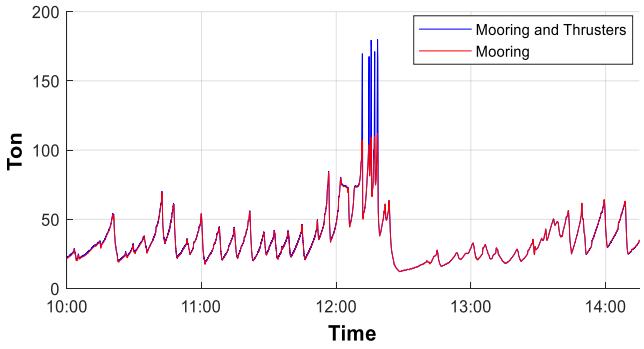

Fig.20 Comparison of extreme mooring force between POT and BM with 0.01 exceeding probability

The highest efficiency of ice management schemes seems to occur for case 3: circle updrift pattern, following by case 4: linear updrift pattern because they provide sharp traces of the icebreaker, which serves to cut the sea ice in the updrift direction as shown in figure 9.

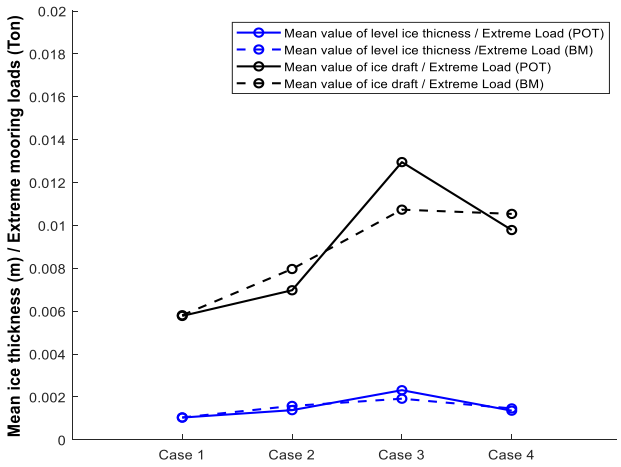

Fig.21 Efficiency of ice management operations by considered extreme loads and ice thickness/draft for level ice and ridges, respectively.

The major factors influencing the IM operations are the level ice thickness, ice draft, ice drift speed and capacity of the icebreaker [8]. Regarding the ice conditions, the ice thickness/draft and ice drift speed can be considered for calculation of the average unit ice momentum in order to estimate the efficiency of the IM operations as demonstrated in figure 22. The unit momentum is calculated from the average mass corresponding to the ice thickness and ice draft multiplied by the average ice drift speed.

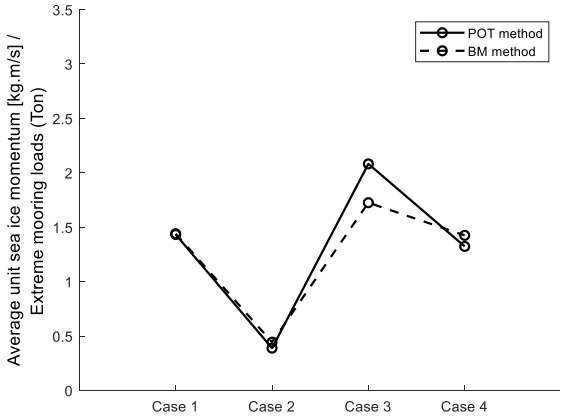

Fig.22 Efficiency of ice management operations by considered average unit sea ice momentum.

It found that the highest efficiency of the IM operations by considering the average unit ice momentum occurs for case 3: circle updrift pattern, which is the same observation of the efficiency of the IM operation as obtained by considering only the ice thickness/draft. However, the efficiency for case 1: square updrift pattern increases when the momentum is considered because the sea ice drifts with the highest speed for this case. This increases the average sea ice momentum. On the other hand, the lowest efficiency of the IM operations occurred for case 2, which is the same observation as for the efficiency of the IM operation by considering only the ice thickness/draft.

The track of the icebreaker for case 2: round circular pattern covers the whole area around the supply vessel, *MV.* Therefore, the efficiency of the ice breaking process in the upstream direction of the ice drift is reduced due to the short traveling distance for which the sea ice is cut. This tends to reduce the efficiency of the IM operation. However, the round circular pattern is of advantage for regions where the ice drift directions are changing rapidly.

The short-term extreme mooring loads estimated by the POT and the BM methods for each IM scheme are normalized by the maximum observed mooring load as illustrated in figure 23. The maximum normalize values took place in case 4: linear updrift pattern with 3.0 and 2.8 for the POT and the BM methods, respectively. Typically, the maximum loads from the simulations of severe environmental conditions are utilized in order to design the mooring system. The results of the normalization implies that there will be a significant increase of the long-term extreme values as compared to the maximum loads observed during short-term operations.

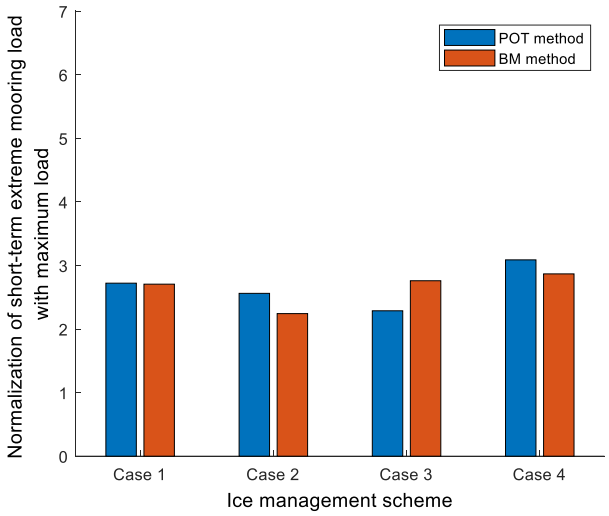

Fig.23 Normalization of extreme value with maximum forces.

Typically, there are several international standards for mooring design such as DNVGL[25], GL Noble Denton[26], American Bureau of Shipping (ABS)[27], Bureau Veritas[28], etc. The safety factors in the international design standards are introduced in order to cover the uncertainty related to the estimated extreme loads and the structural resistance.

In this study, the safety factors are quantified in terms of the reserve strength capacity, calculated as the ratio between the minimum breaking loads, (MBL = 611 ton) of the main mooing chain (76mm type R4) and extreme mooring loading. The reserve strength of the mooring line is approximately 1.9 (MBL, 611ton / maximum extreme mooring load, 320 ton).

It is found that the reserve strength capacity of the main mooring chain is slightly lower than safety factors required by some relevant design standards i.e. DNVGL (S.F. = 1.9), ABS (S.F. = 2.25), GL Noble Denton (S.F. = 1.67), Bureau Veritas (S.F. = 1.67). For longer return periods (e.g. 1-year), this implies that stronger mooring lines should be employed. Moreover, the mooring systems also has a weak link at the load cell and a safety wire, which is able to disconnect in the case of an uncontrollable situation. This also enhances the degree of safety associated with the operation.

Noticeably, the extreme value analysis is essential in the context of mooring system design in order to predict the highest loading that the system will experience during the operation.

CONCLUSION

Short-term extreme value analysis of mooring loads from full-scale measurements for different ice management schemes are investigated. The four different patterns of ice management operations correspond to square updrift, round circle, circle updrift and linear updrift patterns. The associated extreme mooring loads are estimated. During the full-scale experiment, the tension in the mooring line was monitored by a load cell and the measurements were recorded. The peak loads from the resulting time series of mooring load are determined in the present study by peak prominence methods.

The POT and the BM methods are employed in order to estimate the corresponding short-term extreme value distributions. The results of the analysis are quite sensitive to the threshold value for the POT method and to the width of the time window for the BM method. For the BM method, it is found that the Gumbel distribution model provides the best fit to the empirical data for the peak loads. This model is subsequently applied as the parent distribution for the purpose of extreme value analysis. The extreme mooring loads, which are estimated by the two methods for a three-month return period and reduction factor, R due to operation frequency equal to 0.375, agree quite well. The maximum difference between the results obtained by the two methods is about fifteen percent. The uncertainty of the extreme distribution is mainly from the peak mooring loads, which is the consequences of global ice loads on the supply vessel, TV. In this study, the global ice loads were estimated during the IM operations.

The efficiency of the different ice management schemes is quantified by two different measures, i.e. the ratio between the ice thickness/draft and the extreme mooring loads as well as the ratio between the average unit sea ice momentum and the extreme mooring load. The maximum efficiency of the ice management schemes for both of these measures is found for case 3: the circle updrift pattern. This is followed by case 4: the linear updrift pattern. The lowest efficiency occurs for case 2: the round circle pattern.

The minimum reserve strength capacity of the mooring chain during IM operations (with three-month return period and reduction factor, R equal to 0.375) is also compared with the safety factors in relevant design standards, i.e. those of DNVGL, GL Noble Denton, American Bureau of Shipping (ABS) and Bureau Veritas. It is found that the reserve strength (in terms of safety factor) of the mooring chain is 1.9, which is equal to the requirements to the safety factor of DNV GL, slightly lower than the requirements to the safety factor of ABS and higher than the requirements to the safety factor of GL Noble Denton and Bureau Veritas.

However, the mooring systems is equipped with a weak link at load cell (150 ton) and safety wire (223 ton), which implies immediate disconnect in the case of an emergency or uncontrollable situation. The weak link at load cell has a reserve strength capacity of approximately 1.3 times the maximum loads observed during the present IM operations.

Overall, the analysis of extreme mooring loads is essential for the purpose of mooring system design in order to ensure adequate safety and integrity of ships and floating structures during operations in the Arctic

ACKNOWLEDGMENTS

The authors would like to thank all individuals and organizations who have made this study possible. The data from the full-scale measurements was provided by Statoil ASA and Statoil Greenland AS.

This work is supported by the *NTNU Oceans Pilot project Risk, Reliability and Ice Data in Arctic Marine Environments*. Grants from the *Norwegian Ship-owners Association Fund* at NTNU is acknowledged.

REFERENCES

[1] Liferov, P., McKeever, T., Scibilia, F., Teigen, S. H., Kjøl, A., Almkvist, E., and Lindvall, J. K., "Station-keeping trials in ice: Project overview," Proc. ASME 2018 37th International Conference on Ocean, Offshore and Arctic Engineering, American Society of Mechanical Engineers, pp. V008T007A029-V008T007A029.

[2] Serre, N., Kerkeni, S., Sapelnikov, D., Akuetevi, C., Sukhorukov, S., Guo, F., Metrikin, I., and Liferov, P., "Station-Keeping Trials in Ice: Numerical Modelling," Proc. ASME 2018 37th International Conference on Ocean, Offshore and Arctic EngineeringV008T07A022.

[3] ISO, B., 2010, "19906: 2010," Petroleum and natural gas industries–Arctic offshore structures.

[4] Zhao, W., Feng, G., Zhang, M., Ren, H., and Sinsabvarodom, C., 2019, "Effect of low temperature on fatigue crack propagation rates of DH36 steel and its butt weld," Ocean Engineering, p. 106803.

[5] API, R. S., 1996, "Recommended practice for design and analysis of stationkeeping systems for floating structures," American Petroleum Institute.

[6] Veritas, D. N., 2010, "Offshore standard DNV-OS-E301 position mooring," Det Norske Veritas: Høvik, Norway.

[7] Teigen, S. H., Lindvall, J. K., Samardzija, I., and Hansen, R. I., "Station-keeping trials in ice: Ice and metocean conditions," Proc. ASME 2018 37th International Conference on Ocean,

Offshore and Arctic Engineering, American Society of Mechanical Engineers, pp. V008T007A030-V008T007A030.
[8] El Bakkay, B., Coche, E., and Riska, K., 2014, "Efficiency of Ice Management for Arctic Offshore Operations," (45561), p. V010T007A041.
[9] Hamilton, J., Holub, C., Blunt, J., Mitchell, D., and Kokkinis, T., "Ice management for support of arctic floating operations," Proc. OTC Arctic Technology Conference, Offshore Technology Conference.
[10] Neville, M., Almkvist, E., Scibilia, F., Lindvall, J. K., and Liferov, P., "Station-keeping trials in ice: Overview of ice management support," Proc. ASME 2018 37th International Conference on Ocean, Offshore and Arctic Engineering, American Society of Mechanical Engineers, pp. V008T007A027-V008T007A027.
[11] Kjøl, A., Liferov, P., Almkvist, E., Lindvall, J. K., and McKeever, T., "Station-keeping trials in ice: Marine spread," Proc. ASME 2018 37th International Conference on Ocean, Offshore and Arctic Engineering, American Society of Mechanical Engineers, pp. V008T007A023-V008T007A023.
[12] 2017, "Daily test reports of full-scale experiment for station-keeping trials (SKT) in ice ".
[13] Engineering, D.-I., "Trials Data Fitering and Management."
[14] Samardžija, I., 2018, Two Applications of a Cross-Correlation Based Ice Drift Tracking Algorithm; Ship-Based Marine Radar Images and Camera Images from a Fixed Structure.
[15] Nyseth, H., Hansson, A., and Iseskär, J. J., "Station Keeping Trials in Ice: Ice Load Monitoring System," Proc. ASME 2018 37th International Conference on Ocean, Offshore and Arctic Engineering, American Society of Mechanical Engineers, pp. V008T007A031-V008T007A031.
[16] Chai, W., Leira, B. J., and Naess, A., 2018, "Probabilistic methods for estimation of the extreme value statistics of ship ice loads," Cold Regions Science and Technology, 146, pp. 87-97.
[17] Matlab_toolbox, "Findpeaks function of MatLab toolbox," https://ch.mathworks.com/help/signal/ref/findpeaks.html.
[18] Ochi, M. K., 1990, Applied probability and stochastic processes, Wiley New York.
[19] Far, S. S., and Wahab, A. K. A., 2016, "Evaluation of peaks-over-threshold method," Ocean Science Discussions, pp. 1-25.
[20] Goda, Y., 1989, "On the methodology of selecting design wave height," Coastal Engineering 1988, pp. 899-913.
[21] Sinsabvarodom, C., Chai, W., Leira, B. J., Høyland, K. V., and Naess, A., 2019, "Probabilistic Assessment of Ice Rose Diagrams for Ice Drift in the Beaufort Sea," Proceedings of the 25th International Conference on Port and Ocean Engineering under Arctic Conditions.
[22] Suyuthi, A., Leira, B. J., and Riska, K., 2012, "Short term extreme statistics of local ice loads on ship hulls," Cold Regions Science and Technology, 82, pp. 130-143.
[23] Ronkainen, I., Lehtiranta, J., Lensu, M., Rinne, E., Haapala, J., and Haas, C., 2018, "Interannual sea ice thickness variability in the Bay of Bothnia," The Cryosphere, 12, pp. 3459-3476.
[24] Veritas, D. N., "DNV-OS-H101 Marine Operations, General, no. October 2011," Available: h https://rules. dnvgl. com/docs/pdf/DNV/codes/docs/2011-10/Os-H101. pdf i.
[25] DNVGL, 2015, "DNVGL-OS-E301 Position Mooring," DNV GL, Oslo.
[26] Denton, G. N., 2013, "Technical policy board guidelines for moorings, GL noble denton 0032/ND," GL Noble Denton.
[27] ABS, 2018, "Guide for Position Mooring Systems," American Bureau of Shipping Incorporated by Act of Legislature of the State of New York
[28] Veritas, B., 2005, "Classification of Mooring Systems for Permanent and Mobile Offshore Units," Rule Note NR, 493.